

The effects of star-gas interactions on binary evolution in open clusters

JIXUAN YANG(杨季轩) ,¹ LILE WANG(王力乐) ,^{2, 3} XINYU LI(李昕宇) ,¹ MENG SUN(孙萌) ,^{4, 5} AND
 RAINER SPURZEM ,^{4, 6, 2}

¹ Department of Astronomy, Tsinghua University, Beijing 100084, China

² The Kavli Institute for Astronomy and Astrophysics, Peking University, Beijing 100871, China

³ Department of Astronomy, School of Physics, Peking University, Beijing 100871, China

⁴ National Astronomical Observatories, Chinese Academy of Sciences, 20A Datun Road, Chaoyang District, Beijing 100101, China

⁵ Center for Interdisciplinary Exploration and Research in Astrophysics (CIERA), Northwestern University, 1800 Sherman Ave, Evanston, IL 60201, USA

⁶ Astronomisches Rechen-Institut, Zentrum für Astronomie, University of Heidelberg, Mönchhofstrasse 12-14, Heidelberg D-69120, Germany

ABSTRACT

Star-gas interactions can provide gravitational feedback that influences the dynamical evolution of stellar clusters, through processes such as dynamical friction (DF) and its non-dissipative counterpart, negative dynamical friction (NDF). Using the PeTar code, we perform direct N -body simulations of an open cluster initially containing 10^4 stars, evolving within a gaseous medium spanning a range of ambient densities. Our results demonstrate that NDF associated with stellar outflows interacting with the surrounding gas can enhance the rate of cluster expansion, preferentially transporting stars toward the cluster outskirts. This behavior is accompanied by a more rapid decline in the number of binaries composed of a neutron star and a main-sequence star. A statistical analysis of binary orbital parameters further indicates that, compared to DF-dominated evolution, NDF tends to retain systems with larger semi-major axes and lower eccentricities. Outflow-ambient gas interactions can modify the dynamical processing of binaries in star clusters, leading to changes in the survival fraction and composition of the remaining binary population.

Keywords: Stellar dynamics(1596) — Dynamical friction(422) — Open star clusters(1160) — N-body simulations(1083) — Stellar winds(1636) — Interstellar medium(847)

1. INTRODUCTION

Binary star systems play a fundamental role in stellar dynamics, serving as crucial laboratories for understanding multiple astrophysical processes (Tauris & van den Heuvel 2023; Marchant & Bodensteiner 2024; Boffin & Jones 2025). Their evolution drives key mechanisms including mass transfer episodes (Soberman et al. 1997), common-envelope phases (Iben & Livio 1993; Taam & Ricker 2006; Ivanova et al. 2013), Type Ia supernova progenitors (Hillebrandt & Niemeyer 2000;

Wang & Han 2012; Maoz et al. 2014; Livio & Mazzali 2018; Liu et al. 2023), and the formation of exotic objects like blue stragglers (e.g. Mathieu & Latham 1986; Bailyn 1995; Sills 2010; Mathieu & Pols 2025). Furthermore, binary interactions significantly influence planet formation in dense environments (Desidera & Barbieri 2007; Duchêne & Kraus 2013; Kraus et al. 2016) and represent the primary progenitors for gravitational wave (GW) events detected by advanced facilities (Postnov & Yungelson 2014; Abbott et al. 2016; Mapelli 2016; Mandel & Farmer 2022; Mandel & Broekgaarden 2022; Abbott et al. 2023).

There are over $\sim 10^3$ cataloged open clusters (OCs) in the Milky Way (Cantat-Gaudin et al. 2018), providing a statistically rich and dynamically diverse laboratory for studying the evolution of binary populations. Since most stars form in clustered environments (Lada & Lada

Corresponding author: Xinyu Li
 xinyuli@tsinghua.edu.cn

Corresponding author: Meng Sun
 sunmeng@nao.cas.cn

2003), the dynamical processes within OCs can play an important role in shaping binary populations. The relatively high stellar densities in clusters enhance close encounters and dynamical interactions (Antonini et al. 2019); however, the resulting occurrence rates of GW events from compact object mergers in clusters remain debated. While high densities are expected to increase encounter rates, the stochastic nature of cluster dynamics can also produce highly eccentric orbits and eject binaries before merger (see also Bae et al. 2014; Antonini & Rasio 2016; Wendt & Romani 2023). Consistent with this picture, numerical studies have examined the potential contribution of dynamical interactions in open clusters to the formation and evolution of compact binaries relevant for GW sources (Rodriguez et al. 2018; Kumamoto et al. 2019; Rastello et al. 2019).

The interaction between OCs and their ambient interstellar medium (ISM) represents a crucial, yet often overlooked, aspect of cluster evolution. OCs form from giant molecular clouds and experience an early embedded phase, followed by continued interactions with the surrounding gas as they evolve within the Galactic disk (Shu et al. 1987; Kroupa et al. 2001; Lada & Lada 2003; Goodwin & Bastian 2006). During these stages, star-gas interactions can influence the dynamical evolution of clusters. The theoretical foundation for gas dynamical friction (DF) was established by Ostriker (1999), who showed that a gravitating object moving through a gaseous medium experiences a decelerating force due to the formation of an overdense wake. Recent theoretical advances by Gruzinov et al. (2020) and numerical simulations by Li et al. (2020) have revealed that stars with strong outflows can instead generate negative dynamical friction (NDF), whereby an underdense cavity leads to a net acceleration. Such effects are expected to be most relevant for stars with substantial mass loss, particularly during post-main-sequence evolution (Smith 2014).

Understanding how DF and NDF affect binary populations in OCs is crucial for a range of astrophysical contexts. Binary fractions in OCs show significant variation (e.g. Kaczmarek et al. 2011; Jiang et al. 2024), and gas-mediated friction could substantially modify binary formation and dissolution rates. Previous N-body simulations by Liu et al. (2025) investigated OC evolution with gas interactions but were limited by cluster size ($N \sim 1.3 \times 10^3$), yielding insufficient binary statistics for robust analysis. Recent observational studies have begun to characterize binary populations in OCs, including their fractions, orbital properties, and evolutionary outcomes, highlighting the need for larger-scale simulations (Mathieu et al. 2004; Geller et al. 2009, 2015; Geller & Mathieu 2012; Leiner & Geller 2021). Factors influenc-

ing the binary population in clusters and their orbital parameters include cluster-driven dynamical processes, tidal stripping, and gas dynamical effects (Rasio & Heggie 1995; Heggie & Rasio 1996; Fregeau et al. 2009; Leigh et al. 2016; Fragione et al. 2020; Kremer et al. 2020; Ye et al. 2020; González Prieto et al. 2022; Weatherford et al. 2023; Atallah et al. 2024; Kiroğlu et al. 2025). In this work, we focus on the impact of the last channel.

We increase the simulation scale to $N > 10^4$ stars using the `PeTar` N -body code (Wang et al. 2020), with modifications in external force module and stellar evolution module. This larger particle count allows us to retain a statistically significant binary population, enabling detailed analysis of how DF and NDF affect binary parameters, survival rates, and orbital properties across a range of ambient gas densities. Our approach incorporates stellar evolution prescriptions and the respective accelerations from both DF and NDF, providing a systematic investigation of gas-mediated friction effects on binary populations in open clusters.

The paper is organized as follows. In Section 2 we describe the simulation setup and methodology. Section 3 presents the stellar dynamical properties. In Section 4 we focus on the evolution of binary populations under different friction regimes. Section 5 summarizes our main conclusions and discusses their implications.

2. METHOD

2.1. *N*-body Code

We perform numerical simulations using the `PeTar` N -body integrator (Wang et al. 2020) to track the detailed phase-space evolution of each star over 200 Myr during the cluster evolution. The simulations are carried out in a large computational domain (1000 pc on a side), chosen to avoid boundary effects during the cluster evolution.

Our initial conditions are generated using `MCLUSTER` (Küpper et al. 2011), creating an open cluster with 10,000 stars. The stellar mass distribution follows the broken power-law initial mass function of Kroupa (2002), sampled over the mass range 0.2 – $100 M_\odot$, as shown in Figure 1. The lower-mass cutoff is adopted to reduce computational cost while preserving the global dynamical properties of the cluster:

$$\xi(M) \propto \begin{cases} M^{-1.3}, & M < 0.5 M_\odot, \\ M^{-2.3}, & M \geq 0.5 M_\odot. \end{cases} \quad (1)$$

The cluster is initialized with a half-mass radius of 3 pc and follows a King density profile of King (1966) with a concentration parameter $W_0 = 5$, typical of young OCs. There are 2,000 binaries in the initial cluster, cor-

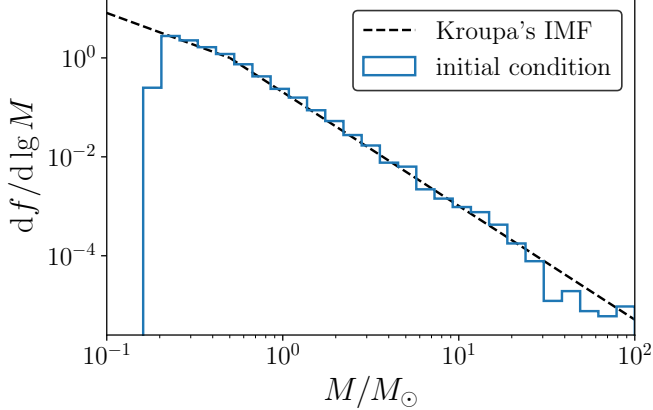


Figure 1. Mass distribution of the initial stellar population in this work. The blue step line shows the sampled initial stellar mass distribution, while the black dashed line indicates the Kroupa (2002) IMF (Eq. (1)), shown in units of $df/d \lg M$.

responding to an initial binary fraction of 40% (Sollima et al. 2010; Donada et al. 2023).

2.2. Dynamical Friction and Negative Dynamical Friction

We implemented both DF and NDF prescriptions within the `PeTar` framework. Stars without significant outflows are assumed to experience the conventional dynamical friction given by Ostriker (1999):

$$a_{\text{DF}} = \frac{4\pi G^2 \rho_0 M}{c_s^2} I_{\text{DF}}(\mathcal{M}), \quad (2)$$

where the acceleration is applied antiparallel to the stellar velocity relative to the gas. The dimensionless function $I_{\text{DF}}(\mathcal{M})$ is given by

$$I_{\text{DF}}(\mathcal{M}) = \frac{1}{\mathcal{M}^2} \times \begin{cases} \ln \left[\Lambda \left(1 - \frac{1}{\mathcal{M}^2} \right)^{1/2} \right], & \mathcal{M} > 1; \\ \frac{1}{2} \ln \left(\frac{1 + \mathcal{M}}{1 - \mathcal{M}} \right) - \mathcal{M}, & \mathcal{M} < 1. \end{cases} \quad (3)$$

Here ρ_0 is the gas density, and $\Lambda \equiv b_{\text{max}}/b_{\text{min}}$ is the Coulomb factor with $b_{\text{max}} = 100$ pc (typical molecular cloud size) and b_{min} is given by the Bondi radius, $r_B = 2GM/c_s^2$. The Mach number $\mathcal{M} \equiv v_*/c_s$ uses the sound speed c_s of the ambient medium, and v_* represents the stellar velocity relative to the ambient gas.

For stars with significant outflows, we implement a prescription for NDF following Gruzinov et al. (2020)

and Li et al. (2020):

$$a_{\text{NDF}} \simeq \pi G \rho_0 \int_0^\pi d\theta \cos \theta \sin \theta R_s \times \left\{ \frac{3}{2} \left[1 + \frac{2u(1 - \cos \theta)}{R_s^2 \sin^2 \theta / R_0^2} \right]^2 - 2 \left[1 + \frac{u^2}{R_s^2 / R_0^2} \right] \right\}. \quad (4)$$

The standoff distance $R_0 = [\dot{m}_w v_w / (4\pi \rho_0 v_*^2)]^{1/2}$ depends on the mass-loss rate \dot{m}_w and wind velocity v_w . The radius of contact discontinuity is $R_s \simeq R_0 [3(1 - \theta \cot \theta) / \sin^2 \theta]^{1/2}$ and velocity ratio is $u \equiv v_*/v_w$. For the low velocity ratios typical in open clusters ($u \ll 1$), this simplifies to $a_{\text{NDF}} \simeq 8.18 G \rho_0 R_0$ (Li et al. 2020).

$$a_{\text{NDF}} = 8.18 G \rho_0 \sqrt{\frac{\dot{m}_w v_w}{4\pi \rho_0 v_*^2}} = 8.18 G \sqrt{\frac{\dot{m}_w v_w \rho_0}{4\pi}} \frac{1}{c_s} I_{\text{NDF}}(\mathcal{M}), \quad (5)$$

$$I_{\text{NDF}}(\mathcal{M}) = \frac{1}{\mathcal{M}}. \quad (6)$$

The resulting acceleration is applied parallel to the stellar velocity relative to the gas.

At sufficiently high stellar velocities, NDF can be suppressed. The critical point is determined by comparing the ambient gas ram pressure $p_0 \sim \rho_0 v_*^2$ with the stellar wind pressure evaluated at the sonic point:

$$p_s = \left(1 + \frac{1}{\gamma} \right) \frac{\dot{m}_w c_{s,w}^5}{\pi G^2 M^2}, \quad (7)$$

where $\gamma = 5/3$ and the wind sound speed is defined as $c_{s,w} = \sqrt{2k_B T_w / m_p}$, with T_w being the wind temperature. When $p_0 \leq p_s$, stellar winds are able to establish a bow shock, leading to the formation of an underdense cavity and the onset of NDF; when $p_0 > p_s$, wind is choked by the ambient medium and the NDF contribution is suppressed, such that I_{NDF} drops to zero. This criterion defines the transition between the active and suppressed NDF regimes in our simulations.

Because the timestep of the `PeTar` integrator depends on the acceleration and its time derivatives up to third order, numerical discontinuities in the force prescription can lead to integration instability. To ensure numerical smoothness across transition regimes, we construct smooth polynomial interpolations for both the DF and NDF kernels. Specifically, we smooth the transition in I_{DF} across $\mathcal{M} = 1$ and the transition in I_{NDF} across $p_0 = p_s$ using tailored polynomial interpolations (including finite negative-order terms where appropriate). In addition, to avoid numerical singularities as $\mathcal{M} \rightarrow 0$, we replace the original expressions for I_{DF} and I_{NDF} (Equations 3 and 6) with fourth-order polynomial expansions

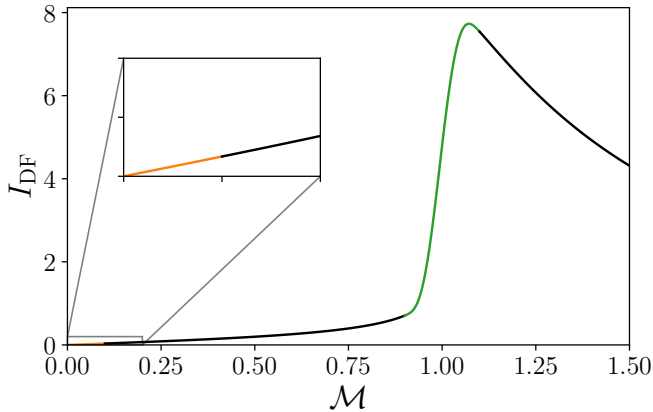


Figure 2. $I_{\text{DF}}(\mathcal{M})$ for $\ln \Lambda = 10$. The black curve shows the analytic expression for I_{DF} given by Equation (3), while the orange and green curves show the polynomial approximations adopted in our simulations to ensure numerical smoothness.

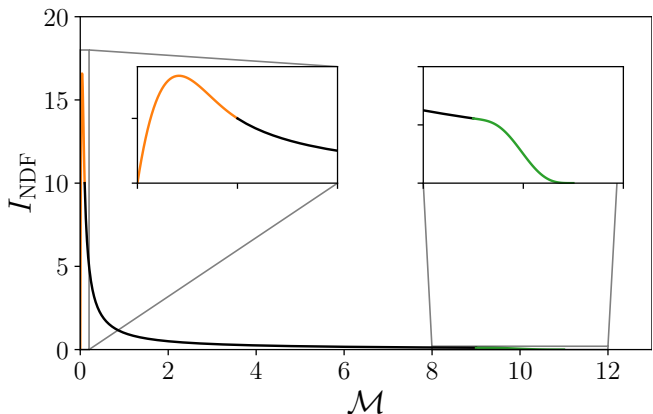


Figure 3. $I_{\text{NDF}}(\mathcal{M})$ for $\mathcal{M}_{\text{crit}} = 10$, where $\mathcal{M}_{\text{crit}}$ is the Mach number at which $p_0 = p_s$. The line styles and colors follow those in Figure 2, with the black curve corresponding to the analytic expression and the colored curves showing the polynomial approximations.

in this limit. All interpolations are constructed such that the acceleration and its first three time derivatives are continuous. The resulting interpolated forms of I_{DF} and I_{NDF} are shown in Figures 2 and 3, respectively.

The characteristic timescale of the gas flow is the Bondi timescale, which is much shorter than the typical dynamical timescales associated with open cluster evolution. We therefore treat DF/NDF accelerations as instantaneous in our simulations. Based on this assumption, we simulate three interaction modes: “NONE” (no gas interactions), “DF” (including only dynamical friction), and “NDF” (including NDF for outflowing stars and DF for stars without significant outflows).

We assume the cluster resides in cold neutral medium (CNM) with $T \simeq 100$ K, $\gamma = 5/3$ and explore gas number densities from $\rho_0 = 30 m_p \text{ cm}^{-3}$ (Milky Way CNM) to $\rho_0 = 3 \times 10^8 m_p \text{ cm}^{-3}$, representing extremely dense gaseous environments. Specifically, we consider $\rho_0 = 30, 300, 3 \times 10^3, 3 \times 10^4, 3 \times 10^6$, and $3 \times 10^8 m_p \text{ cm}^{-3}$.

2.3. Stellar Evolution

We employed a simplified, parameterized stellar evolution model designed to capture the dominant evolutionary stages relevant for mass loss and stellar outflows, rather than to model detailed stellar structure or binary mass transfer. The model includes the main sequence (MS), red giant branch (RGB), and asymptotic giant branch (AGB) phases, followed by transitions to compact objects. The MS lifetime is approximated as $t_{\text{MS}} \simeq 10^{10} \text{ yr} \times (M/M_\odot)^{-2.5}$. The RGB duration is parameterized as

$$t_{\text{RGB}} = \begin{cases} 10^5 \text{ yr} & M > 15 M_\odot \\ 3 \times 10^8 \times (M/M_\odot)^{-4} \text{ yr} , & M \leq 15 M_\odot \end{cases} \quad (8)$$

These scalings are chosen to reproduce the approximate mass dependence of post-main-sequence evolutionary timescales.

Stars with $M < 8 M_\odot$ undergo AGB phases ($\sim 10^5$ yr) before becoming white dwarfs, while more massive stars experience supernovae (SN) ($\sim 10^4$ yr) forming neutron stars ($8 M_\odot \leq M < 25 M_\odot$) or black holes ($M \geq 25 M_\odot$).

We model stellar mass ejection across different evolutionary phases using a simplified, parameterized prescription, with the goal of providing order-of-magnitude outflow properties relevant for NDF, rather than a detailed treatment of stellar wind physics.

For main-sequence stars, we adopt a simple mass-dependent wind prescription to estimate stellar outflows relevant for NDF. The mass-loss rates follow Schröder & Cuntz (2005):

$$\dot{m}_w \simeq 4 \times 10^{-13} M_\odot \text{ yr}^{-1} \times \frac{L}{L_\odot} \frac{R}{R_\odot} \frac{M_\odot}{M}. \quad (9)$$

Using $L \propto M^{3.5}$ (Kuiper 1938) and $R \propto M^{0.8}$ (Demircan & Kahraman 1991) yields $\dot{m}_w \propto (M/M_\odot)^{3.3}$. Wind velocities scale as $v_w = 400 \text{ km s}^{-1} \times (M/M_\odot)^{0.6}$, consistent with solar values and observations of massive O stars. The wind temperatures follow Johnstone et al. (2015):

$$T_w = \frac{2G\bar{\mu}}{\gamma k_B} \left(\frac{c_s}{v_{\text{esc}}} \right)^2 \frac{M_*}{R_*} \sim 2.2 \times 10^6 \text{ K} \times \left(\frac{M}{M_\odot} \right)^{0.2}, \quad (10)$$

Table 1. Summary of simulation parameters

| ID | ρ_0^\dagger (m_p cm $^{-3}$) | Models ‡ | | Description |
|----|--|--------------------|----------|--|
| | | DF | NDF | |
| 0 | 0 | NONE | | No interaction between stars and gas. |
| 1 | 30 | DF-D3E1 § | NDF-D3E1 | CNM in the Milky Way. |
| 2 | 300 | DF-D3E2 | NDF-D3E2 | Dense neutral HI clouds. |
| 3 | 3×10^3 | DF-D3E3 | NDF-D3E3 | Diffuse molecular cloud. |
| 4 | 3×10^4 | * | NDF-D3E4 | Dense molecular cloud cores. |
| 5 | 3×10^6 | * | NDF-D3E6 | Densest molecular cloud cores. |
| 6 | 3×10^8 | * | NDF-D3E8 | AGN-like dense gaseous environment (included for comparison only). |

NOTE— \dagger : ρ_0 is the initial ambient gas density.

\ddagger : DF/NDF denotes dynamical friction / negative dynamical friction models; NONE indicates no gas-star interaction.

\S : The suffix (e.g., D3E1) denotes specific parameter sets.

*: Asterisk indicates that DF simulations were not performed at these densities because the required time steps were prohibitively small.

with a fiducial ratio $c_s/v_{\text{esc}} \sim 0.4$.

For evolved stars, we adopt fiducial outflow parameters. We assume RGB stars have $v_w \approx 30$ km s $^{-1}$, $\dot{m}_w \approx 3 \times 10^{-9} M_\odot$ yr $^{-1}$ and $T_w \sim 1 \times 10^6$ K (Mullan & MacDonald 2019).

The mass-loss rates during the AGB and SN phases are treated as constant and are determined by the difference between the stellar mass at the end of the RGB phase and the final remnant mass. Final remnant masses are $\min\{0.5 M_\odot, 1.0 M_\odot\}$ for WD progenitors, $\min\{0.1 M_\odot, 1.5 M_\odot\}$ for NS progenitors and $5 M_\odot$ for BH progenitors. AGB winds are assumed to have a characteristic velocity $v_w = 30$ km s $^{-1}$ (Ramstedt et al. 2008), while SN ejecta is assigned a characteristic velocity $v_w = 3 \times 10^4$ km s $^{-1}$. Although supernova outflows are intrinsically anisotropic, we neglect natal kicks in order to isolate the effects of NDF, applying a_{NDF} along the instantaneous stellar velocity.

For compact objects, neutron stars eject material at $v_w = 3 \times 10^4$ km s $^{-1}$ (Mor et al. 2023), with the associated $\dot{m}_w \sim 3 \times 10^9 M_\odot$ yr $^{-1}$ and $T_w \sim 10^{8.6}$ K adopted from Paczynski (1990). We neglect WD and BH outflows, as they do not provide significant steady mass loss relevant for NDF.

The adopted outflow parameters for the relevant evolutionary phases are summarized in Table 2. We collectively refer to all mass-ejection processes as outflows for simplicity. This simplified prescription is adopted for computational efficiency and does not affect our qualitative conclusions, which depend primarily on the presence and strength of stellar outflows.

Finally, we assume that the ambient gas density remains uniform and constant in time. This approximation neglects gas removal by supernova feedback and local clearing by binaries, and is adopted to focus on the dynamical impact of DF and NDF under controlled gas conditions.

2.4. Binary Evolution and Analysis

We identify bound stellar pairs by evaluating their total energy in the center-of-mass frame,

$$E_{\text{tot}} = -\frac{Gm_1m_2}{|\vec{r}_1 - \vec{r}_2|} + \frac{m_1m_2(\vec{v}_1 - \vec{v}_2)^2}{2(m_1 + m_2)} . \quad (11)$$

Pairs with $E_{\text{tot}} < 0$ are classified as gravitationally bound. Binary candidates are identified using the `petar.data.process` module. A bound pair is retained as a binary if the two stars are mutual nearest neighbors and their separation is smaller than 5 pc.

For each identified binary, we track the instantaneous orbital parameters, including semi-major axis a , eccentricity e and total system mass M_{tot} . These quantities are computed from the relative positions and velocities of the two components at each output time.

Gas-star interactions are incorporated by applying the DF and NDF acceleration to each component star independently. This treatment assumes that the presence of a binary companion does not strongly modify the local gas response. This approximation is expected to be valid for wide binaries, but may break down for close systems where the binary orbit can perturb the surrounding gas distribution (Wang & Li 2022).

Table 2. Adopted outflow parameters in different evolutionary phases.

| Evolution phase | $\dot{m}_w/(M_\odot \text{ yr}^{-1})$ | $v_w/(\text{km s}^{-1})$ | $T_w/(10^6 \text{ K})$ |
|------------------------|--|--------------------------------|---------------------------------|
| MS | $4 \times 10^{-13} \times (M/M_\odot)^{3.3}$ | $400 \times (M/M_\odot)^{0.6}$ | $2.22 \times (M/M_\odot)^{0.2}$ |
| RGB | 3×10^{-9} | 30 | 1 |
| AGB | † | 30 | * |
| SN ejecta [‡] | † | 3×10^4 | * |
| NS | 3×10^{-9} | 3×10^4 | $10^{2.6}$ |

NOTE— ‡: For the purpose of computing gas-mediated dynamical effects, SN ejecta are treated as an effective outflow.

†: The mass-loss rates during the AGB and SN phases are treated as constant and are determined by the difference between the stellar mass at the end of the RGB phase and the final remnant mass.

*: We assume $p_s \gg p_0$ during the AGB and SN phases. Consequently, we do not explicitly calculate p_s and therefore do not specify the wind temperature in these two phases.

We classify binaries according to their stellar composition: MS–MS, MS–WD, MS–NS, and MS–BH. This classification enables a direct comparison of how different stellar types and their associated outflow properties influence binary survival and orbital evolution under gas-mediated interactions. All stars are initialized as zero-age MS objects at the beginning of the simulation. Over the adopted evolutionary timescale of 200 Myr, the majority of stars remain on the MS, and MS–MS binaries therefore dominate the overall binary population. We place particular emphasis on MS–NS binaries. NS experience strong NDF due to their powerful outflows, making these systems especially sensitive to NDF-driven orbital evolution and disruption. This population is also directly relevant for gravitational wave source demographics (Abbott et al. 2021).

In general, NDF acts to increase binary orbital energy, preferentially disrupting wider systems, whereas DF removes orbital energy and tends to harden bound pairs. We quantify these competing effects statistically by comparing binary populations across a range of ambient gas densities.

3. CLUSTER EVOLUTION AND STELLAR DYNAMICS

3.1. Neutron star expulsion via NDF

We first examine how NDF alters the orbital evolution of NSs in embedded star clusters, and whether it can efficiently remove compact remnants from the cluster independently of supernova kicks. To isolate the role of NDF, we compare simulations with DF-only, NDF, and gas-free (NONE) prescriptions across a range of ambient gas densities.

Figure 4 and 5 show the radial trajectories of stars evolve from MS to NS phase, plotted as a function of time and distance from cluster center. Solid lines denote the trajectories of stars during their MS phase, while dashed lines indicate the post-SN trajectories after the stars have transitioned into NSs. Breaks in the trajectories mark objects that leave the simulation volume.

A clear qualitative difference emerges between simulations that include NDF and those that do not. In the DF-only and gas-free (NONE) runs, most NSs remain confined within the inner few to tens of parsecs over the full 200 Myr evolution, with radial excursions comparable to those of their MS progenitors. By contrast, NDF runs show systematic outward migration of NSs after their formation, with a substantially enhanced fraction of objects reaching large radii or exiting the simulated cluster region.

The efficiency of NS removal via NDF depends strongly on the ambient gas density. At the lowest densities considered (e.g. NDF-D3E1 from Figure 4 top right), only a subset of NSs are driven to large radii within 200 Myr, while others remain temporarily bound. At intermediate densities (e.g. NDF-D3E2–D3E3 from Figure 4 middle and bottom right), outward migration becomes more pronounced and escape events occur more frequently. At the highest densities explored (e.g. NDF-D3E6 and NDF-D3E8 from the third and last panel of Figure 5), nearly all NSs undergo rapid outward displacement, and a significant fraction of massive stars are transported to large radii even before they evolve into compact remnants.

The characteristic timescale for NS displacement shortens systematically with increasing gas density. In the lowest-density NDF runs, NSs typically require \gtrsim

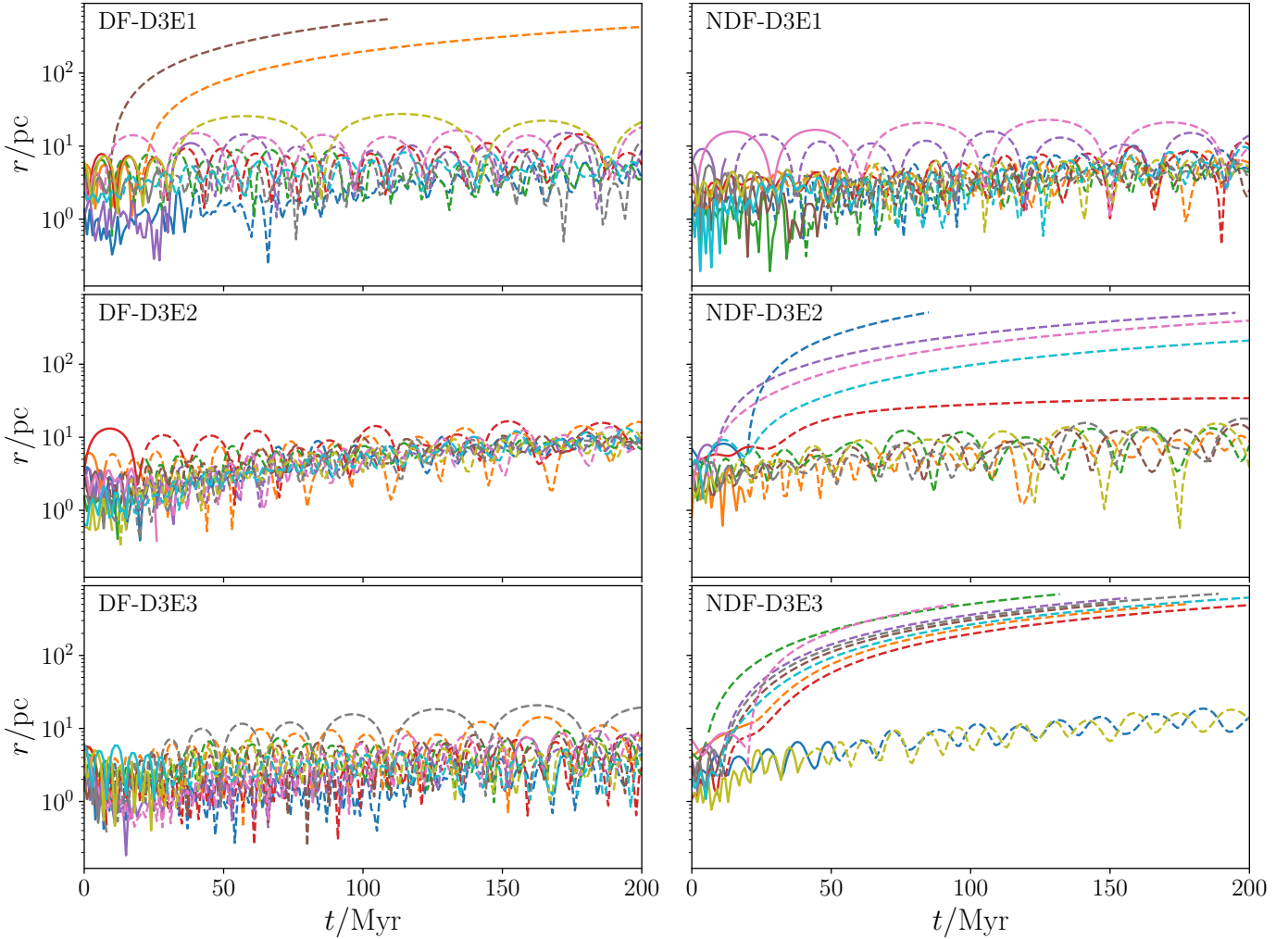


Figure 4. Radial trajectories of stars that transition from the MS phase to the NS phase, shown as a function of time (horizontal axis) and distance from the cluster center (vertical axis). Solid lines represent stellar trajectories during the MS phase, while dashed lines indicate the subsequent trajectories after the stars have become NSs. Only 10 randomly selected trajectories are shown for each simulation for clarity. Breaks in the curves mark objects that leave the simulation volume. Rows correspond to increasing ambient gas density from $30 m_p \text{ cm}^{-3}$ to $3 \times 10^3 m_p \text{ cm}^{-3}$. Columns compare simulations including only DF (left) and those including NDF (right).

100 Myr to reach radii comparable to the size of the simulated cluster region, whereas this timescale decreases to ~ 50 Myr at intermediate densities and to $\lesssim 30$ Myr in the highest-density environments. This behavior reflects the increasing effectiveness of NDF in denser gas, which more rapidly overcomes the gravitational confinement of the cluster in our adopted prescription.

Importantly, the systematic outward migration and loss of NSs in the NDF runs occurs even in the absence of natal SN kicks, demonstrating that NDF provides an efficient and independent channel for removing NSs from young, gas-rich star clusters.

3.2. Distribution of stars in momentum-radius phase space under DF and NDF

To further elucidate how NDF modifies stellar dynamics at the cluster scale, we examine the distribution of stars in momentum-radius phase space. This representation allows us to distinguish between stars that remain gravitationally confined and those undergoing systematic outward acceleration.

As shown in Figure 6, simulations including NDF develop a distinct population of stars at large radii that retain substantial radial momentum. This population is largely absent in the gas-free reference case and becomes increasingly prominent as the ambient gas density increases. The presence of stars with relatively high momentum at large distances indicates that NDF supplies a sustained outward acceleration, preventing efficient deceleration by the cluster potential.

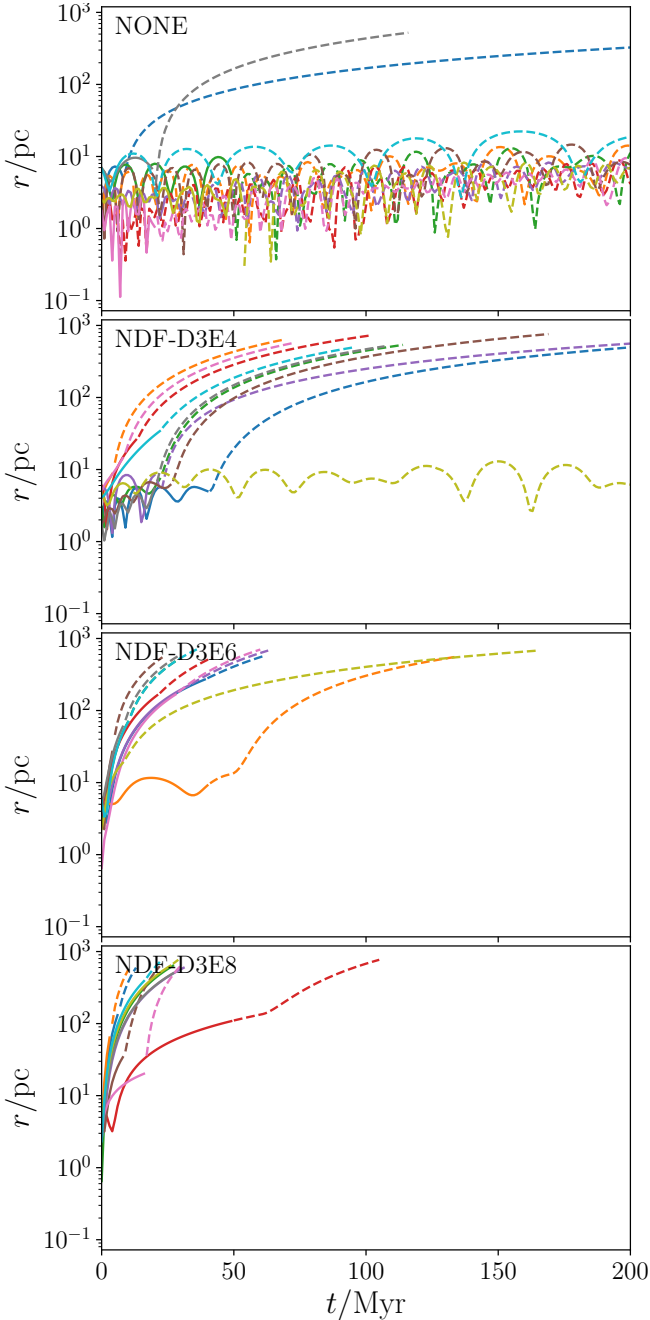


Figure 5. Radial trajectories of stars that transition from the MS phase to the NS phase in simulations with other ambient gas densities than those shown in Figure 4. The layout and line styles follow the same conventions as in Figure 4. Panels labeled NONE show gas-free reference models, while panels labeled NDF-D3E4, NDF-D3E6, and NDF-D3E8 illustrate the effects of NDF in progressively denser environments.

The persistence of this high-momentum, large radius population demonstrates that NDF does not merely perturb stellar orbits locally, but instead reshapes the global phase space structure of the cluster. In denser gas environments, the affected region of phase space expands systematically, consistent with the enhanced efficiency of NDF-driven outward transport observed in the stellar trajectory analysis.

3.3. Radial redistribution of cluster members

A key question for the long-term dynamics of open clusters is whether gas-star interactions can systematically redistribute cluster members in radius, thereby reshaping the global density profile. To quantify this effect, we examine the radial probability density of stars, $f(r) = df/dr$, at two representative epochs, $t = 100$ Myr and 200 Myr, and compare models spanning different gas densities in the DF and NDF modes.

In the absence of gas, as well as in the DF mode, the stellar distribution remains centrally concentrated throughout the evolution, with a pronounced central peak persisting at both epochs. By contrast, clusters evolved in the NDF mode exhibit systematic radial expansion: their radial profiles become progressively shallower, and the peak of $f(r)$ shifts toward larger radii over time.

The strength of this redistribution increases with gas density. In particular, for $\rho = 3 \times 10^6 m_p \text{ cm}^{-3}$, the probability density exceeds that of the no-gas case beyond the second radial bin, indicating efficient outward transport of cluster members driven by non-dissipative gas-star interactions. These trends are summarized in Figures 7 and 8.

3.4. Evolution of cluster scale parameters

The global structural evolution of OCs can be characterized by the time evolution of their characteristic spatial and kinematic scales. In this section, we quantify how gas-star interactions modify cluster expansion and internal kinematics under different interaction regimes.

Across all gas densities, clusters evolved in the NDF mode consistently develop larger characteristic radii than their DF and no-gas counterparts (Figures 9 and 10). This systematic size difference becomes more pronounced at higher gas densities, indicating that non-dissipative gas-star interactions act as an effective heating mechanism that transfers kinetic energy to cluster members and promotes global expansion.

In the DF mode, the half-mass radius increases gradually with time in all models, reflecting the combined effects of two-body relaxation and cluster evaporation. At fixed evolutionary time, increasing gas density leads

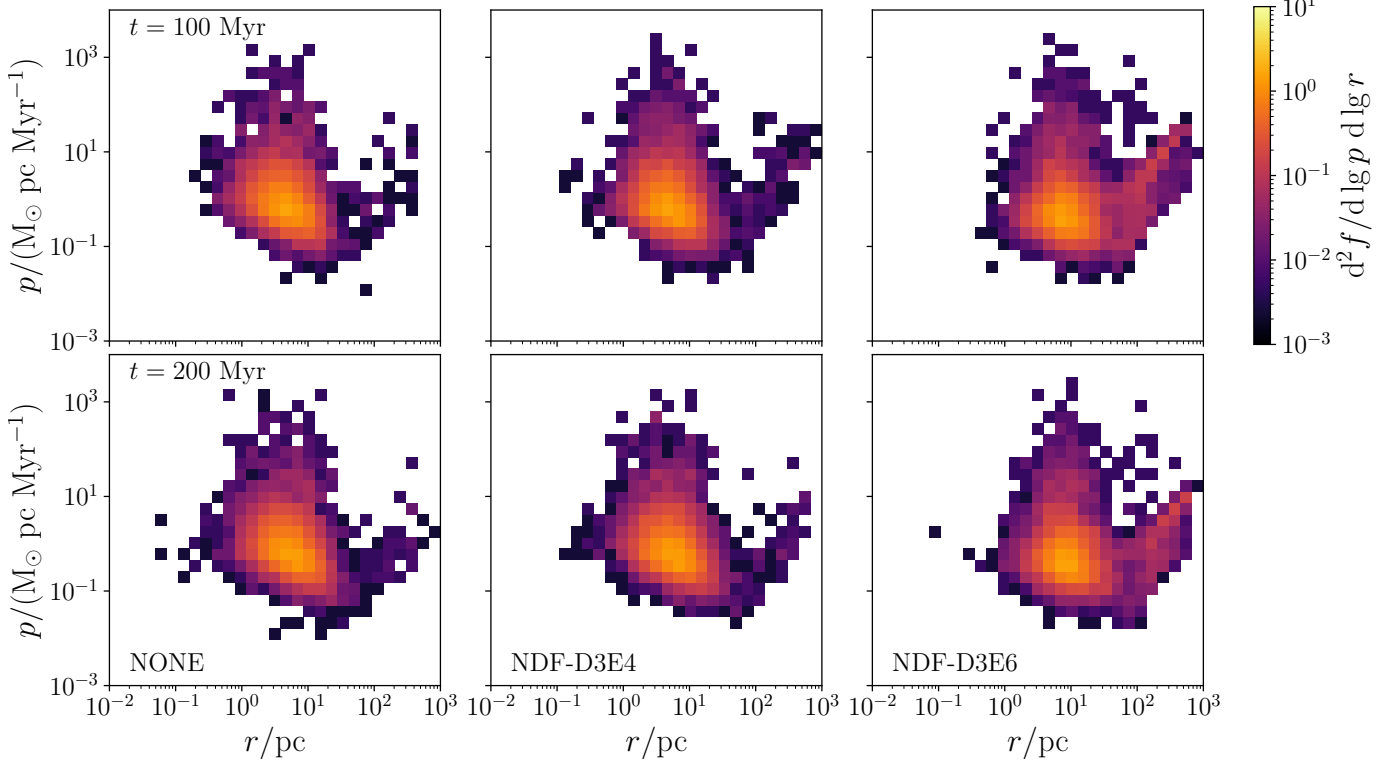


Figure 6. Two-dimensional histograms in momentum–radius phase space. The horizontal axis shows the distance of stars from the cluster center of mass, while the vertical axis shows the stellar momentum. Color indicates the normalized phase-space density. The upper and lower rows present snapshots at $t = 100$ Myr and 200 Myr, respectively. The three columns correspond to simulations with increasing ambient gas density, including a gas-free reference case (NONE) and NDF runs with progressively higher densities.

to smaller half-mass radii and larger velocity scales, as DF extracts orbital energy from stars and suppresses cluster expansion. In intermediate-density environments ($\rho = 3 \times 10^3 m_p \text{ cm}^{-3}$), DF produces slightly more compact configurations than the no-gas case, consistent with the dissipative nature of the interaction. The half-light radius and half-light velocity exhibit larger fluctuations at early time, likely caused by massive stars with short main-sequence lifetimes.

The evolution of the half-light radius differs systematically from that of the half-mass radius, reflecting the mass dependence of cluster dynamics. Because the half-light radius weights stars by luminosity ($L \propto M^{3.5}$), it is more sensitive to the spatial distribution of massive stars. In the DF mode, massive stars experience stronger friction and are preferentially retained in the central regions. As a result, the half-light radius remains relatively small even as the half-mass radius increases, producing a persistent offset between these two scale parameters. This differential behavior provides a potential observational diagnostic of DF-dominated evolution.

Clusters evolved in the NDF mode exhibit qualitatively different behavior. At early times, a pronounced expansion is observed in both the half-mass and half-

light radii for the highest-density model ($\rho = 3 \times 10^6 m_p \text{ cm}^{-3}$). This transient feature is driven by massive MS stars whose strong stellar winds enhance the coupling between the gas and stellar components. Because luminous stars dominate the light budget, the resulting spike is more prominent in the half-light radius than in the half-mass radius.

A similar trend is reflected in the velocity scales. At early times, the half-mass velocity in the $\rho = 3 \times 10^6 m_p \text{ cm}^{-3}$ NDF model exceeds that of lower-density cases, indicating efficient energy injection into the stellar component. As the most massive stars rapidly evolve and collapse into compact objects, this excess kinetic energy is redistributed through relaxation, leading to a subsequent decline in the velocity scale. Because compact remnants do not contribute to the cluster luminosity, the half-light velocity remains relatively high for $\rho = 3 \times 10^6$ and $3 \times 10^8 m_p \text{ cm}^{-3}$, implying that MS stars acquire substantial kinetic energy through non-dissipative gas–star interactions.

4. BINARY DYNAMICS IN CLUSTERS IMMERSED IN GAS

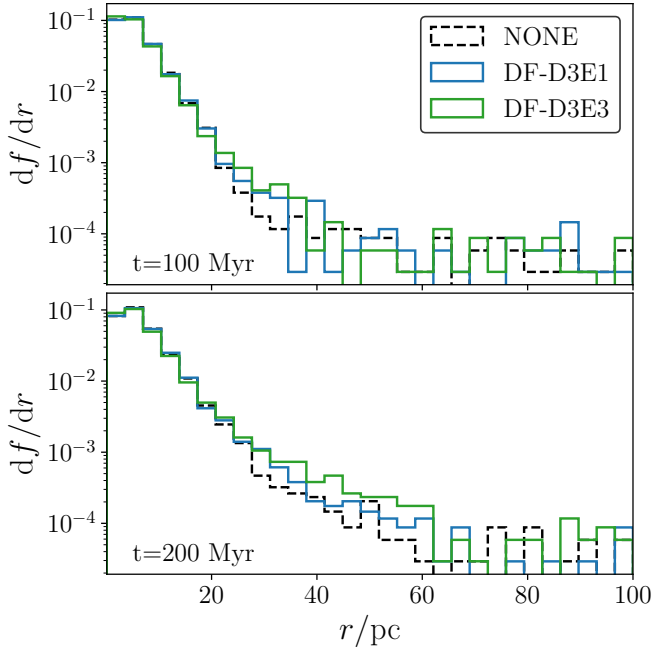


Figure 7. Radial probability density of cluster members in the DF mode for different gas densities. The quantity shown is $f(r) = df/dr$, where $f(r)$ denotes the fraction of stars located within $[r, r + dr]$ from the cluster center. Results are shown at $t = 100$ Myr (upper panel) and $t = 200$ Myr (lower panel). Different colors correspond to different gas densities, while the dashed curve indicates the no-gas case.

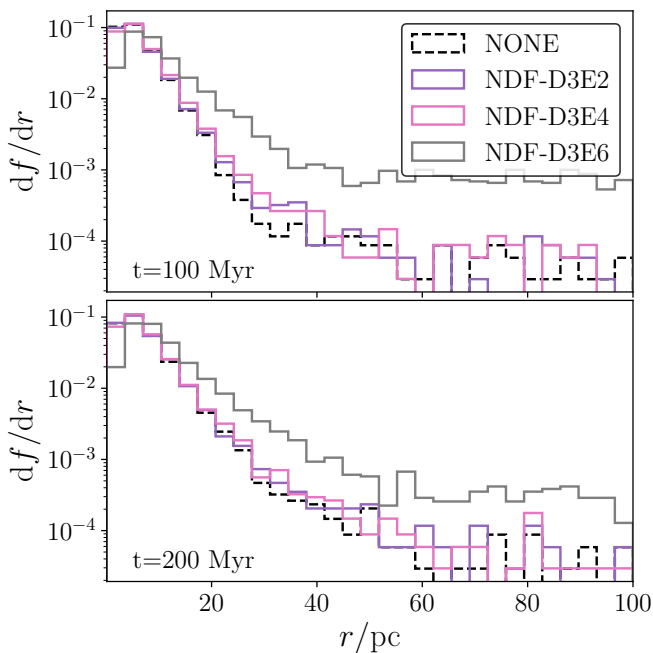


Figure 8. Same as Figure 7, but for the NDF mode.

In this section, we investigate how these gas-star interactions influence the formation, stability, and evolution of binary systems in OCs.

To illustrate the physical scales involved, consider an isolated binary consisting of two MS stars with $m_1 = m_2 = 5 M_\odot$ on a circular orbit with separation $r = 5$ AU. Each star orbits the center of mass with speed

$$v_* = \sqrt{\frac{Gm_1}{2r}} \simeq 21.1 \text{ km s}^{-1}. \quad (12)$$

If the companion outflow sets a local gas density $\rho_0 \simeq \dot{m}/(4\pi r^2 v_w)$ at the location of the accretor, the characteristic NDF acceleration can be estimated as $a_{\text{NDF}} \propto G\rho_0 R_0$ (see Section 2 for the definition of R_0). The corresponding timescale to modify the orbital velocity by order unity is

$$\tau_{\text{NDF}} \sim \frac{v_*}{a_{\text{NDF}}}, \quad (13)$$

which is typically much longer than the $\sim 2 \times 10^6$ Myr lifetime of an open cluster for MS winds and separations of interest. This estimate suggests that, for typical MS binaries, NDF acting in isolation is unlikely to reshape the orbit over the cluster lifetime. In denser gas environments, or for systems embedded in unusually strong outflows, the effect can become non-negligible.

To ensure computational efficiency and avoid the omission of wide pairs, we identify candidate binaries with a maximum separation $s_{\text{max}} = 5$ pc (Section 2.4), followed by our standard boundness criteria. As the separation of widest binary in the cluster is $\sim 10^4$ AU ~ 0.05 pc (Heggie & Hut 2003; Rose et al. 2020), we have also tested $s_{\text{max}} = 0.1$ pc and obtained very similar results, indicating that our conclusions are not sensitive to this choice.

The time evolution of the binary population is summarized in Figure 11. At moderate densities ($\rho = 30$ – $300 m_p \text{ cm}^{-3}$), both DF and NDF have negligible effects on the total number of bound binaries. At higher gas densities, the binary population exhibits a clear mode dependence: DF significantly reduces the number of surviving binaries, whereas NDF increases it. Moreover, the enhancement in the NDF mode becomes increasingly pronounced with increasing gas density.

We classify binaries by their binding energy, $E_b = -E_{\text{tot}} > 0$, where E_{tot} is defined in Eq. (11). Hard binaries are defined as systems whose binding energy exceeds the local average kinetic energy of stars in the cluster ($E_b > \bar{E}_k$), whereas soft binaries have binding energies below the local average kinetic energy ($0 < E_b < \bar{E}_k$) and are therefore easily disrupted by encounters. Heggie’s law (Heggie 1975) states that hard binaries tend

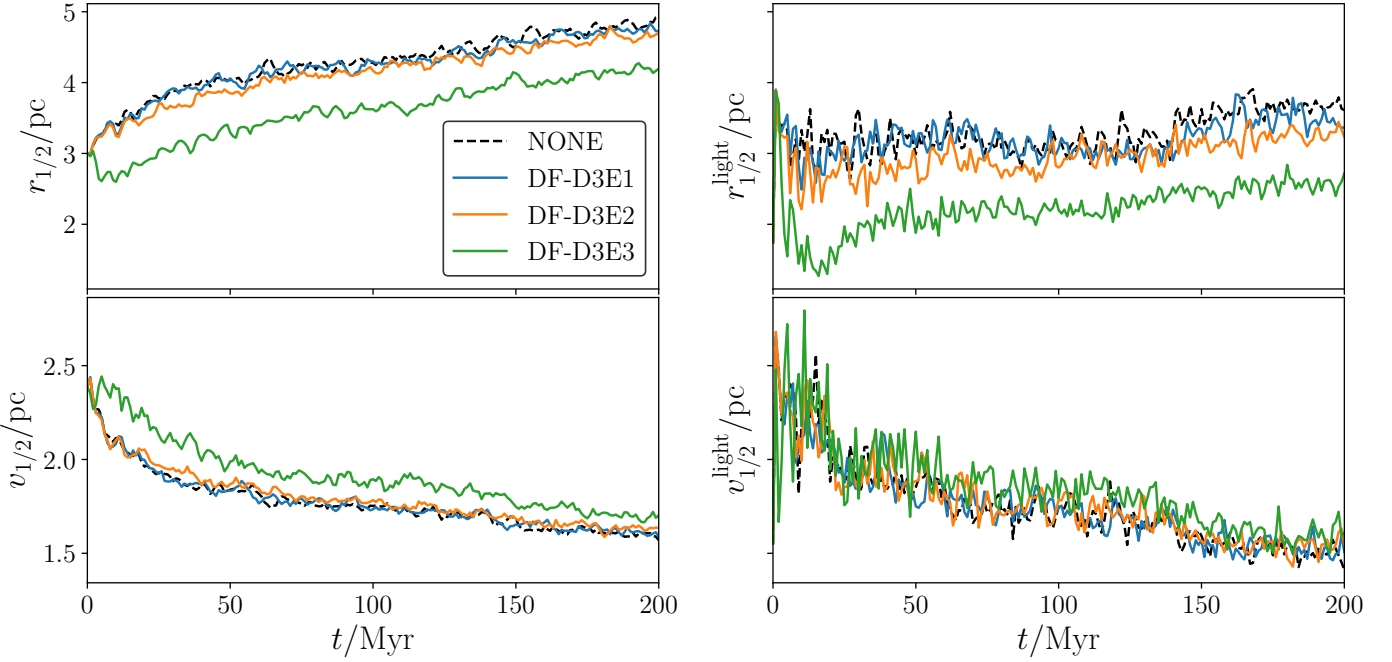


Figure 9. Time evolution of the half-mass radius, half-light radius, and the corresponding velocity scales in the DF mode. Different colors indicate different ambient gas densities, $\rho = 0, 30, 300$, and $3 \times 10^3 m_p \text{ cm}^{-3}$, with the no-gas case shown as a black dashed line.

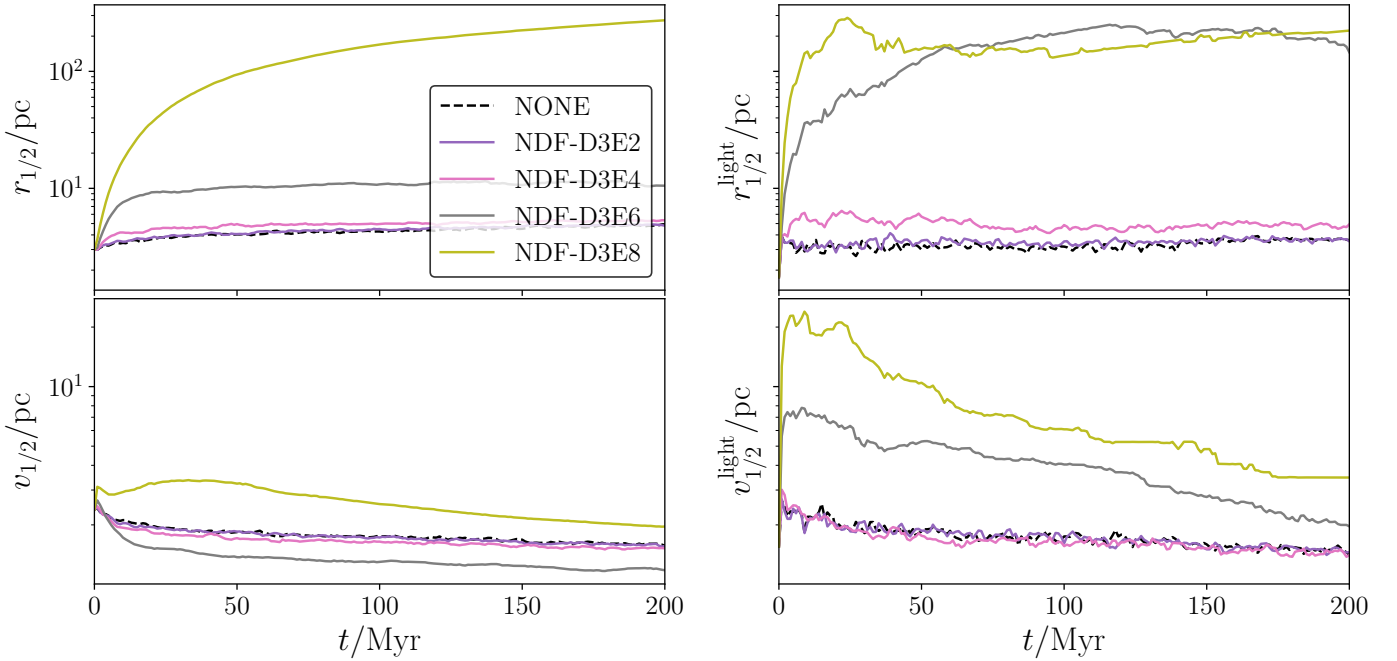


Figure 10. Same as Figure 9, but for the NDF mode. A logarithmic scale is used to accommodate the large dynamical range.

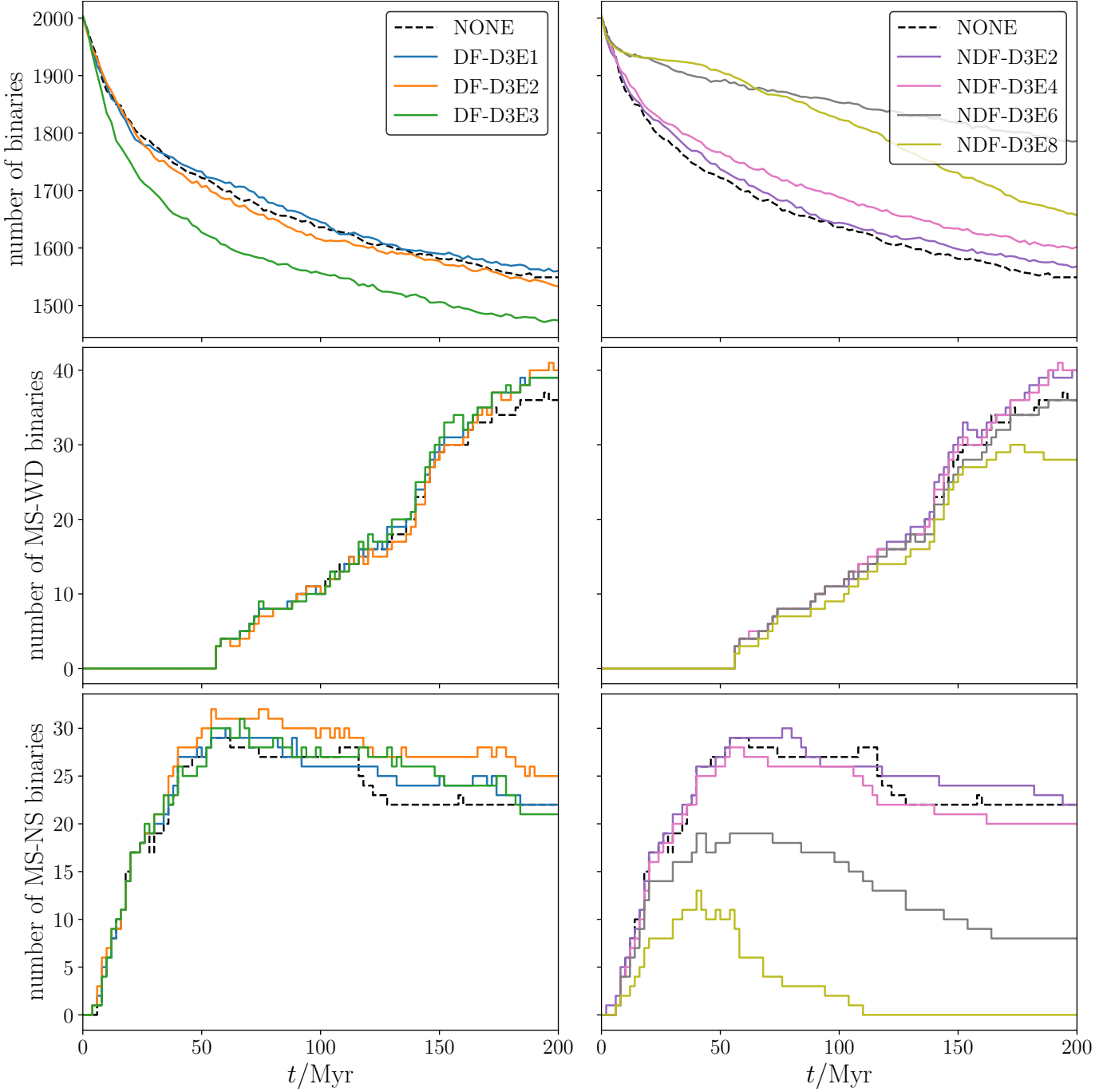


Figure 11. Temporal evolution of the total number of binaries, as well as the numbers of MS-WD and MS-NS binaries in the cluster for different gas densities and interaction models. The left column shows results in DF mode, while the right column shows results in NDF mode. At high gas densities, DF suppresses survival of binaries, while NDF maintains a larger number of surviving binaries.

to become harder and soft binaries tend to become softer as a result of multi-body encounters. DF from the ambient gas is expected to increase the stellar density and encounter frequency, which likely enhances this effect. In contrast, NDF leads to a more diffuse stellar distribution, which may reduce the encounter rate and is consistent with an increased survival probability of soft binaries.

To apply this classification in an inhomogeneous cluster, we estimate the local kinetic energy scale around each binary using the stellar neighborhood of that binary. Specifically, for each binary we select the 100 stars nearest to the binary center of mass and compute the mean kinetic energy of these neighbors

$$\bar{E}_k = \frac{1}{N} \sum_{i=1}^N \frac{1}{2} m_i |\Delta v_i|^2, \quad (14)$$

$$\Delta v_i = v_i - \frac{\sum_N m_i v_i}{\sum_N m_i},$$

where Δv_i is measured relative to the local center-of-mass velocity of the stellar neighborhood surrounding the binary and $N = 100$. The results are insensitive to choosing $N = 50 \sim 200$. This choice provides a practical, spatially local proxy for the typical kinetic energy scale relevant for encounters involving that binary, and avoids relying on a single cluster-averaged velocity scale, which can be misleading once the system develops strong radial gradients in density and velocity dispersion.

Figure 12 shows the temporal evolution of the numbers of soft and hard binaries in our simulations. In DF mode, the number of soft binaries decreases steadily with time. In the DF-D3E3 model, the soft-binary population exhibits a significantly smaller number of soft binaries than both the gas-free case and DF models at lower gas densities. In NDF mode, the number of soft binaries increases with increasing gas density. In the highest-density NDF model, non-dissipative gas-star interactions substantially elevate the local kinetic energy scale, shifting the hard-soft boundary to higher binding energies. As a result, many binaries are reclassified as dynamically soft, resulting in a reduced hard-binary population and an enhanced soft-binary population.

We further classify binaries by their constituent stellar types, including MS-MS, MS-NS, MS-WD, and MS-BH systems (numbers of MS-WD and MS-NS binaries are shown in Figure 11). At low to intermediate gas densities, the number of MS-NS binaries in the DF and NDF model show no significant difference with gas-free model. When $\rho = 3 \times 10^6 m_p \text{ cm}^{-3}$, the number of MS-NS binaries is much lower than in the DF or gas-free models, whereas MS-WD binaries are almost unaffected

by star-gas interaction. In our simulations, NSs are assigned a strong NDF contribution as an effective representation of momentum and energy injection by pulsar winds, which leads to efficient orbital expansion and disruption of MS-NS binaries. In contrast, WDs, which do not produce comparable outflows in our model, are less affected. When gas density goes up to $3 \times 10^8 m_p \text{ cm}^{-3}$, the number of MS-NS binaries become even smaller. The effect of winds in MS phase becomes significant at the highest gas density, resulting in a smaller number of MS-WD binaries than in other NDF models at $t \rightarrow 200 \text{ Myr}$. For the same reason, the number of binaries in NDF-D3E8 becomes smaller than in NDF-D3E6 after $\sim 100 \text{ Myr}$.

Because the MS lifetimes of low mass stars in our simulations (e.g. $\lesssim 1 M_\odot$) are much longer than the total simulation time of 200 Myr, the number of MS-WD binaries continues to grow after $\sim 50 \text{ Myr}$, when the most massive WD progenitors ($\sim 8 M_\odot$) evolve off the MS. In contrast, once the lowest-mass NS progenitors complete their MS evolution, the number of MS-NS binaries ceases to increase. MS-NS binaries are preferentially removed over time by NDF-driven orbital expansion, while MS-WD binaries are more likely to survive and accumulate. This behavior implies that NDF can significantly alter the relative populations of different binary types in OCs, potentially leading to an enhanced abundance of WD binaries relative to NS binaries.

We also analyze the orbital parameters of the surviving binaries, including eccentricity e , semi-major axis a , total mass M_{tot} and orbital inclination i . The distribution of $\cos i$ is essentially uniform, which indicates that the cluster remains nearly spherically symmetric throughout its evolution. e , a and M_{tot} are shown in Figure 13. Results of NDF-D3E6 and NDF-D3E8 show that NDF tends to preserve binaries with larger semi-major axes, producing wider systems, decreasing the binding energy of binary systems. This is demonstrated in the study of a separate binary system (Wang & Li 2022) that outflows in binary systems exert positive torques and expand the orbits. Binaries in NDF-D3E8 also exhibit smaller e and smaller M_{tot} than those in other models. This reflects a preferential disruption of binaries containing more massive stars, which experience stronger non-dissipative interactions in our model. As a result, the surviving binary population is biased toward more circular orbits and lower total masses, reducing the likelihood of stellar collisions and mergers.

These results highlight the dual role of gas in binary evolution: DF tends to suppress the survival of binaries by enhancing stellar encounters, whereas NDF increases the survival probability of wide and soft bina-

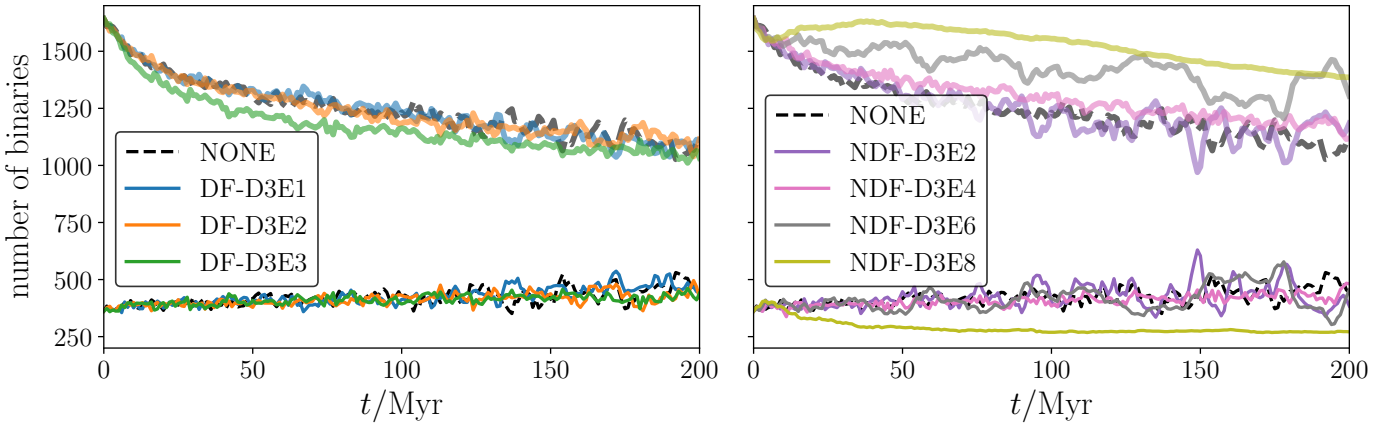


Figure 12. Temporal evolution of the numbers of dynamically soft (thick lines) and hard (thin lines) binaries. Colors denote different ambient gas densities. The left and right panels correspond to models including DF and NDF, respectively.

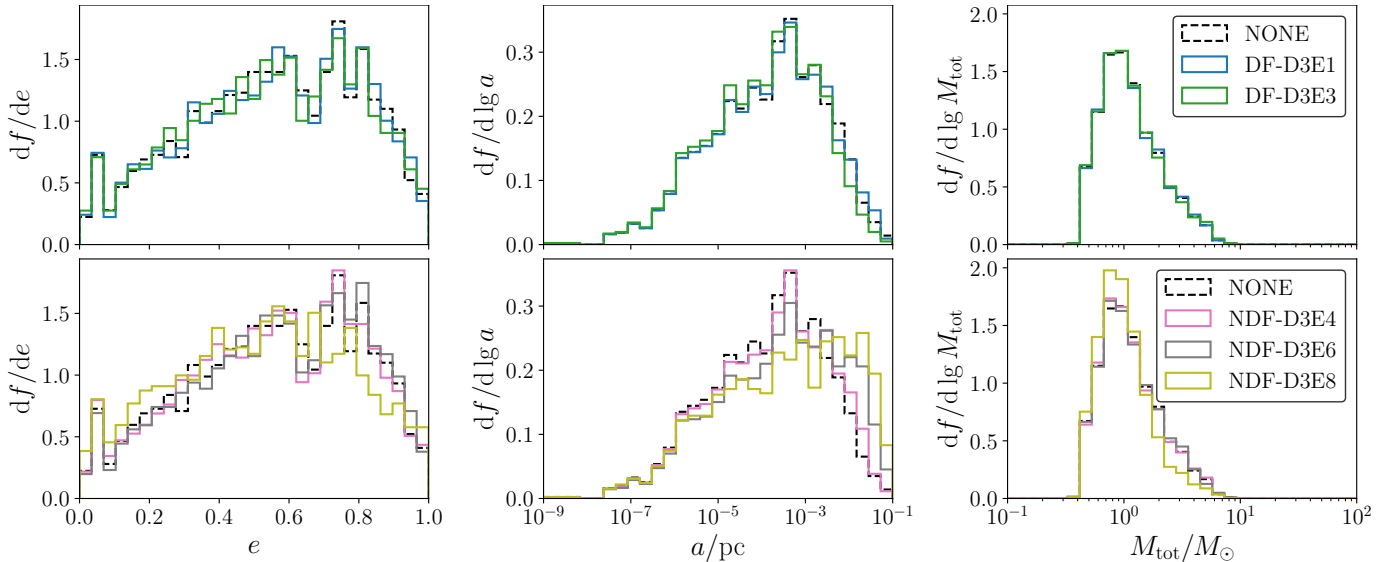


Figure 13. Distributions of orbital parameters for binaries at $t = 200$ Myr in different gas-star interaction models and ambient gas densities. The parameters include eccentricity e (left column), semi-major axis a (middle column) and total mass of binary system M_{tot} (right column).

ries by dynamically heating the cluster and reducing encounter rates. The net outcome depends sensitively on the ambient gas density and on the properties of stellar outflow adopted in the model. In sufficiently dense environments, gas-star interactions may dominate the dynamical evolution of binaries, with potential observational implications for the binary fraction, orbital period distribution, and compact object merger rates in stellar clusters.

5. DISCUSSION AND SUMMARY

This study employs the open-source `PeTar` code to simulate the dynamical evolution of a massive open cluster initially comprising 10,000 stars, and systematically investigating the effects of different gas-star interaction regimes across a wide range of ambient gas densities.

We track both the global structural evolution of the cluster and the detailed behavior of binary populations, with particular attention to systems containing MS stars paired with compact objects (WDs, NSs, and BHs).

The simulations reveal fundamentally contrasting roles of DF and NDF in shaping cluster structure and binary populations. DF drives mass segregation by extracting orbital energy from stars, causing systematic orbital decay and enhanced stellar densities in the cluster core. In contrast, NDF continuously injects kinetic energy into stellar orbits, accelerating cluster expansion and promoting evaporation. Stars subject to NDF migrate outward, producing extended stellar distributions and progressive depletion of the cluster core.

At the binary level, NDF preferentially promotes wider and less tightly bound systems by increasing or-

bial energy, while also tending to circularize orbits. Binary systems containing NSs exhibit the strongest response to NDF. In our simulations, MS–NS binaries decline to nearly zero abundance within ~ 100 Myr at $\rho = 3 \times 10^8 m_p \text{ cm}^{-3}$, reflecting the strong effective NDF acceleration assigned to NSs as a representation of momentum and energy injection by pulsar winds.

The systematic removal of NSs via NDF provides a continuous depletion channel that operates in addition to natal SN kicks. This mechanism may contribute to the observed paucity of NSs in OCs and to their spatial distribution throughout galactic disks. Additionally, the density-dependent acceleration of cluster dissolution suggests that encounters with dense molecular clouds could significantly shorten cluster lifetimes, potentially explaining the rapid disruption observed in some young clusters. The distinctive structural evolution under NDF versus DF, particularly the differential behavior of half-mass versus half-light radii, provides observable signatures that could help identify dominant gas-star interaction mechanisms in real clusters.

The interstellar medium densities explored span from typical Milky Way conditions ($30 m_p \text{ cm}^{-3}$) to extreme environments such as AGN disks ($3 \times 10^8 m_p \text{ cm}^{-3}$). While the latter may not represent typical OC habitats, these high-density simulations serve as controlled scaling experiments that clarify the dependence of gas-star interaction effects on ambient density. The low- to intermediate-density regimes ($30\text{--}300 m_p \text{ cm}^{-3}$), which are more relevant for typical OCs, already demonstrate that gas interactions can significantly influence binary evolution timescales and population demographics.

Our results are broadly consistent with cluster-scale dynamical evolution reported by [Liu et al. \(2025\)](#). An important improvement of the present study is the more robust numerical treatment of the binaries. The relatively low number of surviving binaries in [Liu et al. \(2025\)](#) likely reflects the combined effects of smaller particle numbers, which amplify stochasticity, and the use of integration schemes not optimized for long-term resolution of close encounters. In contrast, `PeTar` is specifically designed for cluster-scale simulations, with accurate handling of binaries, triples, and higher-order systems, leading to improved overall numerical reliability. Consistent with [Liu et al. \(2025\)](#), we find no evidence that NDF universally suppresses the binary population, nor that DF leads to a substantial binary enhancement over the simulation timescales. Our simulations extend these conclusions by resolving how gas-star interactions reshape binary orbital parameters and subtype demographics.

Several caveats accompany our interpretation. The adopted cluster size ($N = 10,000$) exceeds typical OC populations, and approaches the lower end of globular clusters populations, potentially amplifying dynamical effects and binary statistics. The assumption of constant gas temperature ($T = 100$ K) neglects realistic temperature-density correlations and heating from stellar radiation fields, which could modify the effective sound speed and Mach number dependencies in Eq. (2) and (5). Stellar winds, SN explosions, and the gravitational field of stars can also influence the gas density distribution. Uncertainties in stellar evolution prescriptions, particularly wind properties and post-main-sequence mass loss, also propagate directly into the estimated NDF strength.

Finally, our treatment assumes isotropic outflows, whereas real stellar winds and jets are often anisotropic. [Li et al. \(2020\)](#) showed that strongly collimated outflows can suppress or eliminate the NDF effect by preventing the formation of a symmetric underdense cavity. In such cases, the net force remains decelerating, though reduced relative to the standard DF case. The NDF effects reported here should therefore be regarded as upper limits, and the impact of anisotropic outflows warrants dedicated future study.

Although direct observational constraints on the survival boundary of wide and dynamically soft binaries in open clusters remain limited, several lines of evidence suggest that wide systems can exist under specific environmental conditions. High-angular-resolution imaging surveys have revealed the presence of massive companions at separations up to $\sim 10^3\text{--}10^4$ AU in young associations such as Cyg OB2 ([Caballero-Nieves et al. 2014](#)). More generally, multiplicity surveys of nearby star-forming regions show substantial populations of wide systems over separations of $\sim 3\text{--}5000$ AU, providing an empirical baseline for the initial wide-binary inventory prior to significant dynamical processing (e.g., [Kraus et al. 2011](#)). These observations suggest that environmental effects beyond simple stellar-encounter rates may play a role in regulating the survival of soft binaries ([Kraus & Hillenbrand 2007](#)).

ACKNOWLEDGMENTS

The computation resource supporting this work is provided by the KIAA. We thank our colleagues Long Wang and Chuizheng Kong for helpful discussions. We are also grateful to Sanaea Rose for insightful discussions on the dynamical definitions and classification of binary systems.

Software: PeTar (Wang et al. 2020), McLuster (Küpper et al. 2011), numpy (Harris et al. 2020), Matplotlib (Hunter 2007).

REFERENCES

Abbott, B. P., Abbott, R., Abbott, T. D., et al. 2016, PhRvL, 116, 061102, doi: [10.1103/PhysRevLett.116.061102](https://doi.org/10.1103/PhysRevLett.116.061102)

Abbott, R., Abbott, T. D., Abraham, S., et al. 2021, Physical Review X, 11, 021053, doi: [10.1103/PhysRevX.11.021053](https://doi.org/10.1103/PhysRevX.11.021053)

Abbott, R., Abbott, T. D., Acernese, F., et al. 2023, Physical Review X, 13, 041039, doi: [10.1103/PhysRevX.13.041039](https://doi.org/10.1103/PhysRevX.13.041039)

Antonini, F., Gieles, M., & Gualandris, A. 2019, MNRAS, 486, 5008, doi: [10.1093/mnras/stz1149](https://doi.org/10.1093/mnras/stz1149)

Antonini, F., & Rasio, F. A. 2016, ApJ, 831, 187, doi: [10.3847/0004-637X/831/2/187](https://doi.org/10.3847/0004-637X/831/2/187)

Atallah, D., Weatherford, N. C., Trani, A. A., & Rasio, F. A. 2024, ApJ, 970, 112, doi: [10.3847/1538-4357/ad5185](https://doi.org/10.3847/1538-4357/ad5185)

Bae, Y.-B., Kim, C., & Lee, H. M. 2014, MNRAS, 440, 2714, doi: [10.1093/mnras/stu381](https://doi.org/10.1093/mnras/stu381)

Bailyn, C. D. 1995, ARA&A, 33, 133, doi: [10.1146/annurev.aa.33.090195.001025](https://doi.org/10.1146/annurev.aa.33.090195.001025)

Boffin, H. M. J., & Jones, D. 2025, Contributions of the Astronomical Observatory Skalnate Pleso, 55, 21, doi: [10.31577/caosp.2025.55.3.21](https://doi.org/10.31577/caosp.2025.55.3.21)

Caballero-Nieves, S. M., Nelan, E. P., Gies, D. R., et al. 2014, AJ, 147, 40, doi: [10.1088/0004-6256/147/2/40](https://doi.org/10.1088/0004-6256/147/2/40)

Cantat-Gaudin, T., Jordi, C., Vallenari, A., et al. 2018, A&A, 618, A93, doi: [10.1051/0004-6361/201833476](https://doi.org/10.1051/0004-6361/201833476)

Demircan, O., & Kahraman, G. 1991, Ap&SS, 181, 313, doi: [10.1007/BF00639097](https://doi.org/10.1007/BF00639097)

Desidera, S., & Barbieri, M. 2007, A&A, 462, 345, doi: [10.1051/0004-6361:20066319](https://doi.org/10.1051/0004-6361:20066319)

Donada, J., Anders, F., Jordi, C., et al. 2023, A&A, 675, A89, doi: [10.1051/0004-6361/202245219](https://doi.org/10.1051/0004-6361/202245219)

Duchêne, G., & Kraus, A. 2013, ARA&A, 51, 269, doi: [10.1146/annurev-astro-081710-102602](https://doi.org/10.1146/annurev-astro-081710-102602)

Fragione, G., Loeb, A., & Rasio, F. A. 2020, ApJL, 902, L26, doi: [10.3847/2041-8213/abbc0a](https://doi.org/10.3847/2041-8213/abbc0a)

Fregeau, J. M., Ivanova, N., & Rasio, F. A. 2009, ApJ, 707, 1533, doi: [10.1088/0004-637X/707/2/1533](https://doi.org/10.1088/0004-637X/707/2/1533)

Geller, A. M., Latham, D. W., & Mathieu, R. D. 2015, AJ, 150, 97, doi: [10.1088/0004-6256/150/3/97](https://doi.org/10.1088/0004-6256/150/3/97)

Geller, A. M., & Mathieu, R. D. 2012, AJ, 144, 54, doi: [10.1088/0004-6256/144/2/54](https://doi.org/10.1088/0004-6256/144/2/54)

Geller, A. M., Mathieu, R. D., Harris, H. C., & McClure, R. D. 2009, AJ, 137, 3743, doi: [10.1088/0004-6256/137/4/3743](https://doi.org/10.1088/0004-6256/137/4/3743)

González Prieto, E., Kremer, K., Fragione, G., et al. 2022, ApJ, 940, 131, doi: [10.3847/1538-4357/ac9b0f](https://doi.org/10.3847/1538-4357/ac9b0f)

Goodwin, S. P., & Bastian, N. 2006, MNRAS, 373, 752, doi: [10.1111/j.1365-2966.2006.11078.x](https://doi.org/10.1111/j.1365-2966.2006.11078.x)

Gruzinov, A., Levin, Y., & Matzner, C. D. 2020, MNRAS, 492, 2755, doi: [10.1093/mnras/staa013](https://doi.org/10.1093/mnras/staa013)

Harris, C. R., Millman, K. J., van der Walt, S. J., et al. 2020, Nature, 585, 357, doi: [10.1038/s41586-020-2649-2](https://doi.org/10.1038/s41586-020-2649-2)

Heggie, D., & Hut, P. 2003, The Gravitational Million-Body Problem: A Multidisciplinary Approach to Star Cluster Dynamics

Heggie, D. C. 1975, MNRAS, 173, 729, doi: [10.1093/mnras/173.3.729](https://doi.org/10.1093/mnras/173.3.729)

Heggie, D. C., & Rasio, F. A. 1996, MNRAS, 282, 1064, doi: [10.1093/mnras/282.3.1064](https://doi.org/10.1093/mnras/282.3.1064)

Hillebrandt, W., & Niemeyer, J. C. 2000, ARA&A, 38, 191, doi: [10.1146/annurev.astro.38.1.191](https://doi.org/10.1146/annurev.astro.38.1.191)

Hunter, J. D. 2007, Computing in Science and Engineering, 9, 90, doi: [10.1109/MCSE.2007.55](https://doi.org/10.1109/MCSE.2007.55)

Iben, Jr., I., & Livio, M. 1993, PASP, 105, 1373, doi: [10.1086/133321](https://doi.org/10.1086/133321)

Ivanova, N., Justham, S., Chen, X., et al. 2013, A&A Rv, 21, 59, doi: [10.1007/s00159-013-0059-2](https://doi.org/10.1007/s00159-013-0059-2)

Jiang, Y., Zhong, J., Qin, S., et al. 2024, ApJ, 971, 71, doi: [10.3847/1538-4357/ad5344](https://doi.org/10.3847/1538-4357/ad5344)

Johnstone, C. P., Güdel, M., Lüftinger, T., Toth, G., & Brott, I. 2015, A&A, 577, A27, doi: [10.1051/0004-6361/201425300](https://doi.org/10.1051/0004-6361/201425300)

Kaczmarek, T., Olczak, C., & Pfalzner, S. 2011, A&A, 528, A144, doi: [10.1051/0004-6361/201015233](https://doi.org/10.1051/0004-6361/201015233)

King, I. R. 1966, AJ, 71, 64, doi: [10.1086/109857](https://doi.org/10.1086/109857)

Kiroğlu, F., Kremer, K., & Rasio, F. A. 2025, ApJL, 994, L37, doi: [10.3847/2041-8213/ae1eeb](https://doi.org/10.3847/2041-8213/ae1eeb)

Kraus, A. L., & Hillenbrand, L. A. 2007, ApJ, 662, 413, doi: [10.1086/516835](https://doi.org/10.1086/516835)

Kraus, A. L., Ireland, M. J., Huber, D., Mann, A. W., & Dupuy, T. J. 2016, AJ, 152, 8, doi: [10.3847/0004-6256/152/1/8](https://doi.org/10.3847/0004-6256/152/1/8)

Kraus, A. L., Ireland, M. J., Martinache, F., & Hillenbrand, L. A. 2011, ApJ, 731, 8, doi: [10.1088/0004-637X/731/1/8](https://doi.org/10.1088/0004-637X/731/1/8)

Kremer, K., Ye, C. S., Rui, N. Z., et al. 2020, *ApJS*, 247, 48, doi: [10.3847/1538-4365/ab7919](https://doi.org/10.3847/1538-4365/ab7919)

Kroupa, P. 2002, *Science*, 295, 82, doi: [10.1126/science.1067524](https://doi.org/10.1126/science.1067524)

Kroupa, P., Aarseth, S., & Hurley, J. 2001, *MNRAS*, 321, 699, doi: [10.1046/j.1365-8711.2001.04050.x](https://doi.org/10.1046/j.1365-8711.2001.04050.x)

Kuiper, G. P. 1938, *ApJ*, 88, 472, doi: [10.1086/143999](https://doi.org/10.1086/143999)

Kumamoto, J., Fujii, M. S., & Tanikawa, A. 2019, *MNRAS*, 486, 3942, doi: [10.1093/mnras/stz1068](https://doi.org/10.1093/mnras/stz1068)

Küpper, A. H. W., Maschberger, T., Kroupa, P., & Baumgardt, H. 2011, *MNRAS*, 417, 2300, doi: [10.1111/j.1365-2966.2011.19412.x](https://doi.org/10.1111/j.1365-2966.2011.19412.x)

Lada, C. J., & Lada, E. A. 2003, *ARA&A*, 41, 57, doi: [10.1146/annurev.astro.41.011802.094844](https://doi.org/10.1146/annurev.astro.41.011802.094844)

Leigh, N. W. C., Stone, N. C., Geller, A. M., et al. 2016, *MNRAS*, 463, 3311, doi: [10.1093/mnras/stw2178](https://doi.org/10.1093/mnras/stw2178)

Leiner, E. M., & Geller, A. 2021, *ApJ*, 908, 229, doi: [10.3847/1538-4357/abd7e9](https://doi.org/10.3847/1538-4357/abd7e9)

Li, X., Chang, P., Levin, Y., Matzner, C. D., & Armitage, P. J. 2020, *MNRAS*, 494, 2327, doi: [10.1093/mnras/staa900](https://doi.org/10.1093/mnras/staa900)

Liu, M., Wang, L., Fu, X., & Ho, L. C. 2025, *ApJ*, 978, 87, doi: [10.3847/1538-4357/ad91a9](https://doi.org/10.3847/1538-4357/ad91a9)

Liu, Z.-W., Röpke, F. K., & Han, Z. 2023, *Research in Astronomy and Astrophysics*, 23, 082001, doi: [10.1088/1674-4527/acd89e](https://doi.org/10.1088/1674-4527/acd89e)

Livio, M., & Mazzali, P. 2018, *PhR*, 736, 1, doi: [10.1016/j.physrep.2018.02.002](https://doi.org/10.1016/j.physrep.2018.02.002)

Mandel, I., & Broekgaarden, F. S. 2022, *Living Reviews in Relativity*, 25, 1, doi: [10.1007/s41114-021-00034-3](https://doi.org/10.1007/s41114-021-00034-3)

Mandel, I., & Farmer, A. 2022, *PhR*, 955, 1, doi: [10.1016/j.physrep.2022.01.003](https://doi.org/10.1016/j.physrep.2022.01.003)

Maoz, D., Mannucci, F., & Nelemans, G. 2014, *ARA&A*, 52, 107, doi: [10.1146/annurev-astro-082812-141031](https://doi.org/10.1146/annurev-astro-082812-141031)

Mapelli, M. 2016, *MNRAS*, 459, 3432, doi: [10.1093/mnras/stw869](https://doi.org/10.1093/mnras/stw869)

Marchant, P., & Bodensteiner, J. 2024, *ARA&A*, 62, 21, doi: [10.1146/annurev-astro-052722-105936](https://doi.org/10.1146/annurev-astro-052722-105936)

Mathieu, R. D., & Latham, D. W. 1986, *AJ*, 92, 1364, doi: [10.1086/114269](https://doi.org/10.1086/114269)

Mathieu, R. D., Meibom, S., & Dolan, C. J. 2004, *ApJL*, 602, L121, doi: [10.1086/382686](https://doi.org/10.1086/382686)

Mathieu, R. D., & Pols, O. R. 2025, *ARA&A*, 63, 467, doi: [10.1146/annurev-astro-071221-054402](https://doi.org/10.1146/annurev-astro-071221-054402)

Mor, R., Livne, E., & Piran, T. 2023, *MNRAS*, 518, 623, doi: [10.1093/mnras/stac2775](https://doi.org/10.1093/mnras/stac2775)

Mullan, D. J., & MacDonald, J. 2019, *ApJ*, 885, 113, doi: [10.3847/1538-4357/ab4658](https://doi.org/10.3847/1538-4357/ab4658)

Ostriker, E. C. 1999, *ApJ*, 513, 252, doi: [10.1086/306858](https://doi.org/10.1086/306858)

Paczynski, B. 1990, *ApJ*, 363, 218, doi: [10.1086/169332](https://doi.org/10.1086/169332)

Postnov, K. A., & Yungelson, L. R. 2014, *Living Reviews in Relativity*, 17, 3, doi: [10.12942/lrr-2014-3](https://doi.org/10.12942/lrr-2014-3)

Ramstedt, S., Schöier, F. L., Olofsson, H., & Lundgren, A. A. 2008, *A&A*, 487, 645, doi: [10.1051/0004-6361:20078876](https://doi.org/10.1051/0004-6361:20078876)

Rasio, F. A., & Heggie, D. C. 1995, *ApJL*, 445, L133, doi: [10.1086/187907](https://doi.org/10.1086/187907)

Rastello, S., Amaro-Seoane, P., Arca-Sedda, M., et al. 2019, *MNRAS*, 483, 1233, doi: [10.1093/mnras/sty3193](https://doi.org/10.1093/mnras/sty3193)

Rodriguez, C. L., Amaro-Seoane, P., Chatterjee, S., et al. 2018, *PhRvD*, 98, 123005, doi: [10.1103/PhysRevD.98.123005](https://doi.org/10.1103/PhysRevD.98.123005)

Rose, S. C., Naoz, S., Gautam, A. K., et al. 2020, *ApJ*, 904, 113, doi: [10.3847/1538-4357/abc557](https://doi.org/10.3847/1538-4357/abc557)

Schröder, K. P., & Cuntz, M. 2005, *ApJ*, 630, L73, doi: [10.1086/491579](https://doi.org/10.1086/491579)

Shu, F. H., Adams, F. C., & Lizano, S. 1987, *ARA&A*, 25, 23, doi: [10.1146/annurev.aa.25.090187.000323](https://doi.org/10.1146/annurev.aa.25.090187.000323)

Sills, A. 2010, in *American Institute of Physics Conference Series*, Vol. 1314, *International Conference on Binaries: in celebration of Ron Webbink's 65th Birthday*, ed. V. Kalogera & M. van der Sluys (AIP), 105–112, doi: [10.1063/1.3536351](https://doi.org/10.1063/1.3536351)

Smith, N. 2014, *ARA&A*, 52, 487, doi: [10.1146/annurev-astro-081913-040025](https://doi.org/10.1146/annurev-astro-081913-040025)

Soberman, G. E., Phinney, E. S., & van den Heuvel, E. P. J. 1997, *A&A*, 327, 620, doi: [10.48550/arXiv.astro-ph/9703016](https://doi.org/10.48550/arXiv.astro-ph/9703016)

Sollima, A., Carballo-Bello, J. A., Beccari, G., et al. 2010, *MNRAS*, 401, 577, doi: [10.1111/j.1365-2966.2009.15676.x](https://doi.org/10.1111/j.1365-2966.2009.15676.x)

Taam, R. E., & Ricker, P. M. 2006, *arXiv e-prints*, astro, doi: [10.48550/arXiv.astro-ph/0611043](https://doi.org/10.48550/arXiv.astro-ph/0611043)

Tauris, T. M., & van den Heuvel, E. P. J. 2023, *Physics of Binary Star Evolution. From Stars to X-ray Binaries and Gravitational Wave Sources*, doi: [10.48550/arXiv.2305.09388](https://doi.org/10.48550/arXiv.2305.09388)

Wang, B., & Han, Z. 2012, *NewAR*, 56, 122, doi: [10.1016/j.newar.2012.04.001](https://doi.org/10.1016/j.newar.2012.04.001)

Wang, L., Iwasawa, M., Nitadori, K., & Makino, J. 2020, *MNRAS*, 497, 536, doi: [10.1093/mnras/staa1915](https://doi.org/10.1093/mnras/staa1915)

Wang, L., & Li, X. 2022, *ApJ*, 932, 108, doi: [10.3847/1538-4357/ac6ce6](https://doi.org/10.3847/1538-4357/ac6ce6)

Weatherford, N. C., Kiroğlu, F., Fragione, G., et al. 2023, *ApJ*, 946, 104, doi: [10.3847/1538-4357/acbcc1](https://doi.org/10.3847/1538-4357/acbcc1)

Wendt, D. K., & Romani, R. W. 2023, *ApJ*, 944, 112, doi: [10.3847/1538-4357/abc64a](https://doi.org/10.3847/1538-4357/abc64a)

Ye, C. S., Fong, W.-f., Kremer, K., et al. 2020, *ApJL*, 888, L10, doi: [10.3847/2041-8213/ab5dc5](https://doi.org/10.3847/2041-8213/ab5dc5)